ISSN 2616-5775 Vol. 6, Issue 13: 178-185, DOI: 10.25236/AJCIS.2023.061325

Prediction of Sunspot Activity Cycle Based on Long Short-Term Memory (LSTM) Network Models

Yilin Jiang[1,†], Yufei Xiong[1,†]

[1]*Southwest University of Political Science and Law, Chongqing, China*
[†]*These authors also contributed equally to this work.*

Abstract: *This paper addresses the prediction of sunspot activity using cycle feature analysis and Long Short-Term Memory Network (LSTM) models, including LSTM-NN. Analysis of sunspot data since 1700 reveals a 100-year major cycle and an 11-year minor cycle, with findings indicating the current 25th solar cycle began in December 2019 and ends in January 2031, and the 26th cycle from January 2031 to January 2041, both resembling the low activity levels of the 24th cycle. Employing a multivariate construction method, the study combines LSTM with univariate and multivariate predictions in single and multi-time steps, with the optimal strategy determined by the minimum root-mean-square error. The multivariable model predicts the peak of the next cycle in November 2035, lasting until May 2037, a duration of 1 year and 6 months.*

Keywords: *Sunspot Prediction, Cycle Feature Analysis, Long Short-Term Memory Network (LSTM), Multivariate Model*

1. Introduction

Sunspots, a key indicator of solar activity, exhibit an 11-year cyclical pattern on the sun's surface. Their fluctuating numbers are closely tied to solar outbursts, which can disrupt Earth's magnetic field, affect communication systems, and indirectly influence climate change. Predicting these cycles, particularly the maximum amplitude and timing, is essential for understanding future solar activities and their impact on Earth. This paper focuses on developing mathematical models to accurately predict sunspot patterns using publicly available data from observatories and space science research organizations. Our objectives include forecasting the start, end, and peak periods of the current and upcoming solar cycles, providing insights into the interplay between solar activities and Earth's climate[1-2].

2. Prediction of the Beginning and End of Current and Next Solar Cycles

2.1 Research Methods

The relative sunspot number data is from the website of Space Environment Prediction Center of National Space Science Center of Chinese Academy of Sciences (http://www.sepc.ac.cn/). There have been complete annual records of sunspots since 1700, monthly records since 1749, and daily records since 1818. The annual record of sunspots has a history of 318 years. This paper uses year records for sunspot data before 1749, and month records for data after 1749. The day records were compiled into month records quickly before the official release of the month records, so as to participate in the application practice of prediction.

This paper employs wavelet analysis to examine the relative number of long-term sunspots. Wavelet analysis, based on wavelet and Fourier transforms, is a potent period analysis tool. Introduced by French geophysicist Morlet in 1983, it is adept at multi-scale analysis. Through wavelet transform preprocessing, characteristic information is effectively extracted from discrete observational data. The core of this method involves the continuous wavelet change function, defined for a given wavelet function across time series. Particularly, the Morlet wavelet function and its associated coefficients play a crucial role in this analysis. The wavelet square difference, computed over time domains, forms the basis of the wavelet difference graph, a key instrument in determining the primary periods of the series.

The historical process similarity of relative sunspot numbers is identified using goodness of fit and

ISSN 2616-5775 Vol. 6, Issue 13: 178-185, DOI: 10.25236/AJCIS.2023.061325

the Nash efficiency coefficient. This approach aims to forecast sunspot numbers from 2019 to 2030. The goodness of fit, represented by the coefficient of determination R2, assesses the congruence between regression values and observed data. The closer R2 is to 1, the better the fit. Conversely, lower R2 values indicate poorer fitness. The Nash efficiency coefficient, conceptualized by Nash and Sutcliffe in 1970, is a dimensionless parameter assessing the accuracy of calculated values against target values. Its efficacy is indicated by values ranging from -∞ to 1, with higher positive values denoting better simulation effects. In this study, the Nash efficiency coefficient is used to evaluate the fitting degree between observed and estimated values, providing a clear measure of the model's predictive accuracy[3-5].

2.2 Sunspot activity cycle analysis

Wavelet analysis method was used to analyze the relative annual average of 318a sunspots from 1700 to 2017, and the results were shown in Figure 1 and Figure 2.

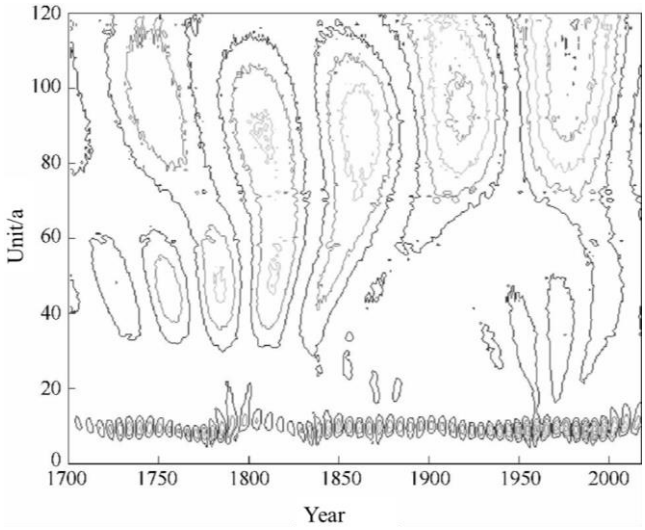

Figure 1: Real part of the wavelet transform coefficient

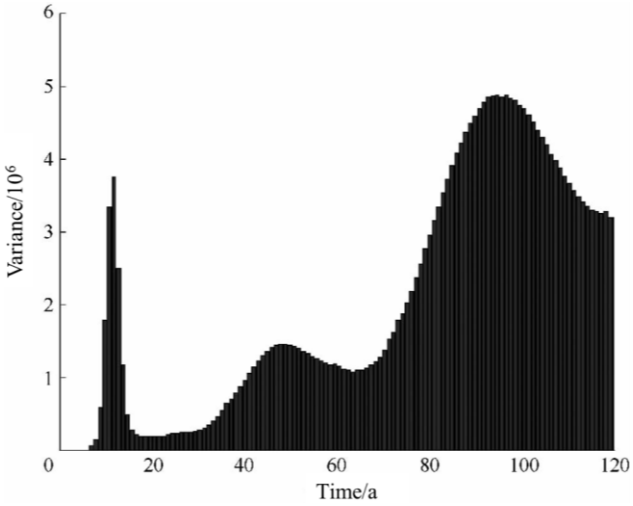

Figure 2: Wavelet square difference

As can be seen from the contour line of the real part of the wavelet coefficient in Figure 1, there are two periodic evolution rules of the relative number of sunspots, which are about 8 ~ 11a and 96 ~ 102a. In Figure 2, there are two peaks in the wavelet square difference curve, and the maximum peak corresponds to a time scale of about 98a, indicating that the oscillation period of this time scale is the strongest, and it is the first main period of the relative sunspot number sequence. The second largest peak is about 10a time scale, which is the second main period of the series.

According to the year of relative sunspot number valley value to the next valley value year is 1 sunspot cycle, it can be concluded that each "100a" cycle contains 9 small cycles, and the statistical results are listed in Table 1.

ISSN 2616-5775 Vol. 6, Issue 13: 178-185, DOI: 10.25236/AJCIS.2023.061325

Table 1: Statistics of sunspot "100a" large cycle characteristics

Cycle number	Time/year - month	Large week Time length /a	Small cycle average length /a	Average relative number of sunspots	Maximum relative sunspot number	Minimum relative sunspot number
1	1712-01-1811-06	99.5	11.06	46.27	154.4	0
2	1811-07-1913-06	102	11.33	42.78	138.3	1.4
3	1913-07-2009-07	96.08	10.68	65.72	189.9	2.6

According to the statistical results in Table 1, the average length of small cycles in the first 100a cycle is 11.06a; In the second 100a large cycle, the average length of small cycles is 11.33a; In the third 100a large cycle, the average length of the small cycle is 10.68a. During the 100a large cycle, the average length of the small cycle is larger. The average length of all the small periods in the three 100a large cycles is 11.02, which shows that the sunspot has a 11a small period rule[6-8].

It can be found from Figure 3 that there are 2 to 3 continuous low-value small cycle rules during the 100a big week. Since 1700, there have been 3 major cycles, and in between the 3 major cycles, there are 2 to 3 low-value minor cycles. In front of the first "100a" major cycle, there were two consecutive low-value small cycles from 1700 to 1723. Since there was no record of the relative number of sunspots before 1700, it is impossible to prove whether there were three consecutive low-value small cycles. There were three consecutive low-value small periods between the first and second 100a cycles, from August 1798 to June 1833; And there were three consecutive low-value minor cycles between the second and third 100a major cycles, from September 1878 to June 1913. The statistical rules of successive low-value small periods between the "100a" major cycles are listed in Table 2. The average relative number of sunspots in each low-value small period is smaller than the average relative number of sunspots in the "100a" major cycle.

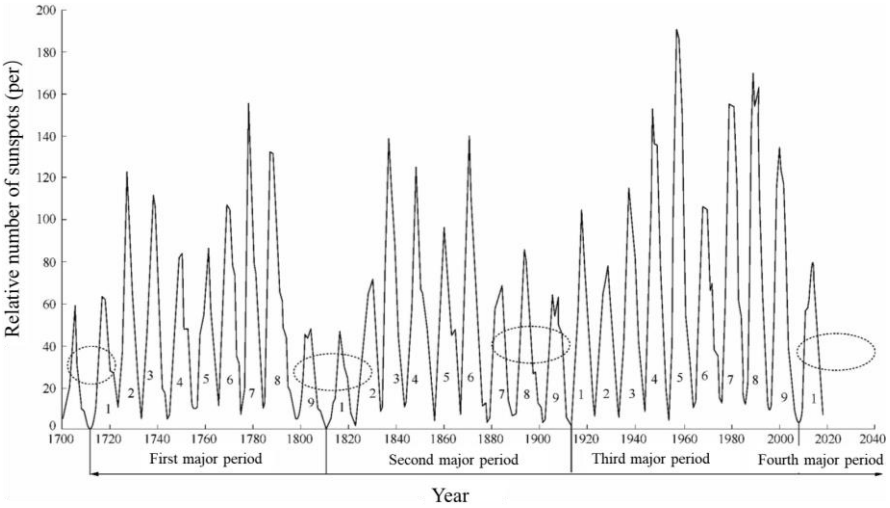

Figure 3: Process line of relative sunspot number of 300a

Table 2: Statistics of sunspot 11a small period characteristics

The number of large periods of 100a	11a Number of large cycles	Rising segment /a	Drop section /a	Cycle length /a	Start time/year - month	End Time Valley Year/year - month	Sunspot average
0	9	6.25	6.67	12.92	1798-08	1811-06	16.8
1	1	4.75	7.67	12.42	1811-07	1823-11	28
1	9	6.42	3.17	9.58	1823-12	1833-06	22
2	1	3.67	7.58	11.25	1878-09	1889-11	18.9
2	2	3.75	8.67	12.42	1889-12	1902-04	41.2
2	7	4.83	6.33	11.17	1902-05	1913-06	34.4
2	8	4.58	6.67	12.92	2009-08	1811-06	37.3
2	9	6.25	7.67	12.42	1798-08	1823-11	33.1
4	1	4.75	1811-07				

ISSN 2616-5775 Vol. 6, Issue 13: 178-185, DOI: 10.25236/AJCIS.2023.061325

2.3 Prediction of sunspot activity cycle trend

This research examines the sunspot activity cycle rule since 1700, identifying that since August 2009, we have been in the first minor cycle of the fourth centennial cycle, a period marked by historically low sunspot values. Key low-value mini-cycles, including those from 1700, 1712, 1798, 1811, 1824, 1878, 1890, and 1902, are analyzed as reference samples. Using the goodness of fit method and the Nash-Sutcliffe efficiency coefficient, the study identifies the 1902, 1824, and 2009 series as having the most similar sunspot patterns to the current cycle. Particularly, the period from May 1902 to June 1913 is concluded to be the most analogous to the cycle beginning in August 2009. This conclusion is based on a detailed analysis of each cycle's length, the duration of rising and falling segments, and the average, maximum, and minimum values of relative sunspot numbers. The recognition results, summarized in a table, present a comparative view of historical periods, highlighting the 1902 series with the highest R2 value of 0.88 and a Nash-Sutcliffe efficiency coefficient of 0.83, indicating its close similarity to the current cycle.

According to the analysis of sunspot activity cycle characteristics and the fitting results of the most similar section in history, the sunspot phase similarity period from 1996 to 2020 is from 1889 to 1913. According to the characteristics of similar years, the following trend conclusions can be drawn.

(1) As shown in Figure 4, the 25th cycle begins in December 2019. From then on, solar activity begins to slowly increase and then fall back, until around January 2031, when the current cycle ends.

(2) As shown in Figure 5, the sunspots of cycle 26 of the next cycle will start in January 2031, and the relative number of sunspots will show the lowest value of the cycle around January 2041, thus ending the cycle.

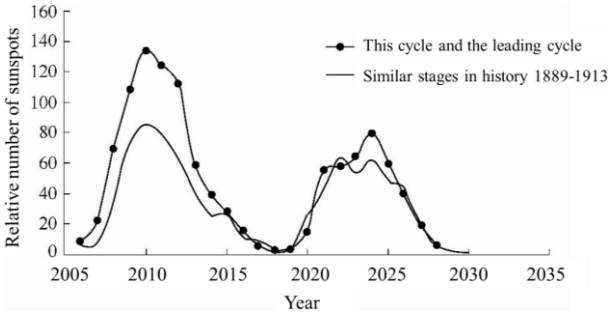

Figure 4: Fitting the most similar segment of the history of sunspot processes in this cycle (Cycle 25)

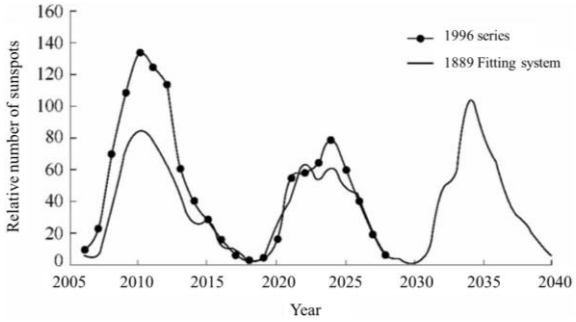

Figure 5: Fitting the most similar segment of the sunspot process history for the next cycle (cycle 26)

3. Prediction of the Beginning and Duration of the Solar Maximum in the Next Solar Cycle

3.1 Research Methods

Sunspot data using SILSO website (http://www.sidc.be/silso/datafiles) sunspot released version 2.0 of 13 months smooth monthly data (Source: WDC - SILSO Royal Observatory of Belgium, Brussels). 270 years, from June 1749 to March 2019, with 3,237 data sets, Figure 6.1, where the horizontal coordinate is the start date of each solar cycle, derived from 13 months of smoothed monthly data for sunspots, Released on SILSO website is recorded in the sunspot cycle (http://sidc.oma.be/silso/cvcesmm). For example, Cycle 1 ran from February 1755 to May 1766 and Cycle 2 ran from June 1766 to May 1775.

ISSN 2616-5775 Vol. 6, Issue 13: 178-185, DOI: 10.25236/AJCIS.2023.061325

The 13-month smoothed monthly sunspot number is referred to as the monthly smoothed sunspot number for short in Figure 6.

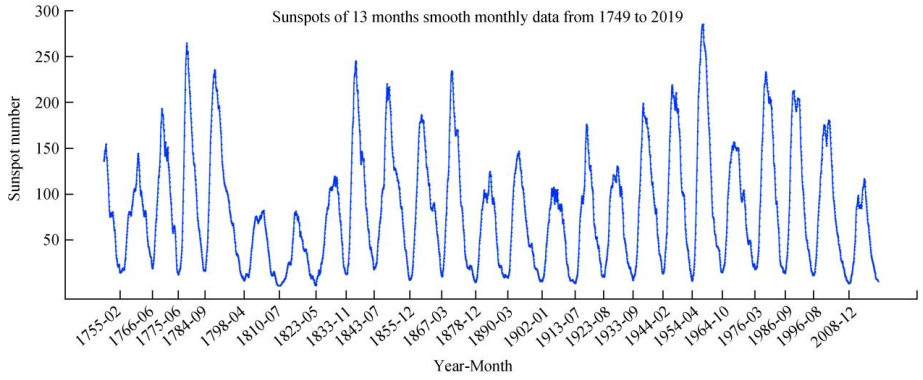

Figure 6: Smoothed monthly sunspot observations for 13 months.

The rapid advancement in neural networks has led to the widespread adoption of Long Short-Term Memory (LSTM) networks in the field of deep learning. Distinguished from basic neural networks, LSTM networks excel in processing time series data by establishing weight links both between and within layers. As a type of recurrent neural network (RNN) tailored for sequence-based data, LSTM networks adeptly handle the evolution of sequences and reveal intricate relationships within them. A critical advantage of LSTM networks is their ability to counteract the gradient vanishing issue commonly encountered in RNNs when processing long sequence data, making them particularly apt for tasks that involve significant time lapses, such as speech recognition, machine translation, and time series prediction. The LSTM network's working unit integrates the information input of the current moment with the hidden state and cell state of the previous moment, employing three gates for information processing: the forgetting gate, input gate, and output gate (as illustrated in Figure 7). These gates collectively manage the persistence and suppression of information. The forget gate uses the sigmoid activation function to regulate the retained information from the previous state. The input gate, comprising a sigmoid function and tanh activation function, creates a candidate vector value that contributes to the current cell state. Finally, the output gate generates the current hidden state and conveys it to the subsequent units. The layered structure of the LSTM network, depicted in Figure 8, demonstrates how each layer processes and passes on the data. In a multi-time-step network model, the LSTM processes the time series in multiple data segments, with each unit contributing distinct weights, thereby enhancing the time correlation of the data. This multi-step approach provides a richer context for time series analysis, as it incorporates diverse weight links and multiple information correlations within the response process.

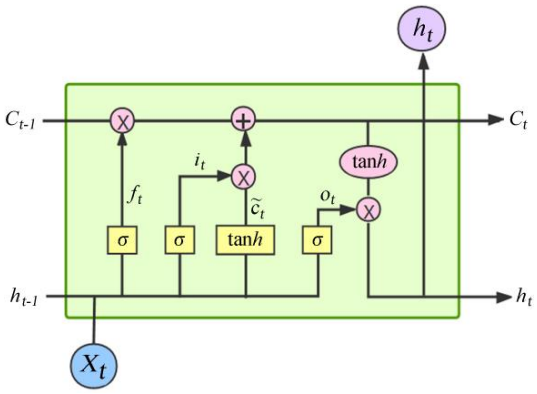

Figure 7: LSTM cell

ISSN 2616-5775 Vol. 6, Issue 13: 178-185, DOI: 10.25236/AJCIS.2023.061325

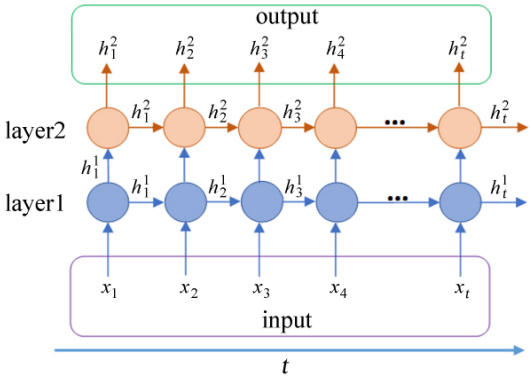

Figure 8: LSTM network layers

In LSTM network applications, the setting of the time step is crucial. A time step of 1 implies that a single unit handles the input and output, establishing basic information persistence in the time series data. However, with multiple time steps, different units provide varying weights, creating a more complex network where information persistence is established both within individual units and across interconnected units, enhancing the temporal correlation of the data. To evaluate the effectiveness of multi-step methods and determine the optimal step size, a strategy involving multiple step and lag combinations is employed. Here, steps are set as divisors of 120 to align with the goal of predicting monthly trends over a 120-month period. The varying combinations of step lengths and lag numbers, including single-step predictions (step length of 1, lag number of 120) and 15 different multi-step configurations, are analyzed. This approach allows for a nuanced exploration of how different time intervals affect prediction accuracy, providing a comprehensive understanding of the most effective LSTM network configurations for time series forecasting.

This study extends traditional univariate prediction methods by introducing a multivariate approach to sunspot prediction. In addition to using sunspot data, the model incorporates the length of the sunspot cycle as an additional input, thereby increasing the dimensionality of the data. This method involves pairing observed sunspot values with their corresponding positions in the cycle, effectively capturing both the value and the cycle's relative position. For example, in a cycle with 135 observed sunspots, a sequence from 0 to 134 is created alongside the sunspot values, accounting for both the value and the length of the cycle[9-10].

To retain the temporal dependence of observations, the study employs continuous subsequence sampling using a sliding window technique within the sunspot time series. This creates multiple continuous subsequences, each modeled individually to assess development strategies against observed data. The dataset is divided into two groups: Shard 11 with 11 subsequences and Shard 6 with 6 subsequences. Each subsequence is further split into a training set for model training and a test set for model evaluation, providing a comprehensive structure for analyzing the LSTM network model's performance.

The verification of the model's predictions is crucial for establishing reliability. The same model, with consistent hyperparameters, is applied to each subsequence within the dataset. The prediction accuracy is evaluated based on the root-mean-square error (RMSE) between the model's predictions and the observed values for each subsequence. The mean RMSE across all subsequences is then calculated to determine the overall effectiveness of the prediction model. This approach, involving an average of 11 RMSEs from the sampled subsequences, offers a holistic measure of the model's predictive capability on the complete sunspot time series dataset.

3.2 Experimental results and analysis

Pytorch framework is used as the development model, two network layers and 50 hidden units are used in the design of long short-term memory network, Adam is used as the optimizer and MAE is used as the loss function. Visdom tool was used to detect the convergence of the loss function in real time. The model was trained in 100 cycles in total.

Combined with the sampling methods above, the prediction effect of all step schemes in univariate and multivariate was compared. The mean value of root means square error of all subsequences (AVG) and standard deviation of root means square error of all subsequences (STD) were used to illustrate the results, respectively.

ISSN 2616-5775 Vol. 6, Issue 13: 178-185, DOI: 10.25236/AJCIS.2023.061325

First, the prediction effect of single variable in the asynchronously long strategy is compared, including single step prediction and 15 kinds of multi-step prediction. Table 3 shows the mean root mean square error of Shard 11 and Shard 6 in single step prediction and optimal multi-step prediction respectively. In the multi-step experiment with 8 steps and 15 lags in Shard 11, the mean value of the lowest RMS error is 43.1, which is 1.9 lower than that of 45.0 for the single step prediction, and the standard deviation is reduced from 20.2 to 19.1. For the multi-step experiment with 5 steps and 24 lags in Shard 6, the mean value of the lowest root-mean-square error is 50.4, which is 3.1 lower than the 53.5 predicted by single step, but the standard deviation is increased from 16.6 to 18.1.

Table 3: Univariate results of 11-slice and 6-slice in single-step and optimal multi-step

Methods			Subsequence											AVG	STD
			1	2	3	4	5	6	7	8	9	10	11		
11-Slice	Univariate	Multi-step	47.9	35.9	66.9	54.7	27.8	22	29.8	54.8	29.1	33.3	92.6	45	20.2
		Single step	49.9	31.6	68	35.2	16.6	31.8	33.7	46.2	36.9	34.8	89.1	43.1	19.1
6-Slice	Univariate	Multi-step	50.7	28.3	43.5	53.8	62.4	82.4	-	-	-	-	-	53.5	16.6
		Single step	48.4	24.6	37.6	50.1	58.6	83.2	-	-	-	-	-	50.4	18.1

The multivariate prediction also compares the effects of the single-step and multi-step methods. Table 4 shows the mean root-mean-square error of Shard 11 and Shard 6 in the single-step prediction and optimal multi-step, respectively. The minimum RMS error obtained by Shard 11 with multi-step size of 6 and lag number of 20 is 42.8, which is 2.6 lower than 45.4 for single-step prediction, and the standard deviation is 15.6, which is 8.0 lower than 23.6 for single-step prediction. Shard 6 has a MMS error of 51.6 for steps of 12 and lags of 10, which is 3.5 less than the single step prediction of 55.1, and the standard deviation increases from 20.1 to 23.4.

Finally, the optimal strategies of Shard 11 and Shard 6, namely 6 steps of multivariate and 5 steps of univariate, were used to predict the number of sunspots in the next 10 years respectively. The results are shown in Figure 9. In Shard 11, the maximum amplitude of solar cycle 25 is 144.9, which occurs in December 2022; And the maximum amplitude of solar Cycle 25 in Shard 6 is 180.4, which occurs in May 2024.

Table 4: Multivariate results for 11-slice and 6-slice at a single-step and optimal multi-step results

Methods			Subsequence											AVG	STD
			1	2	3	4	5	6	7	8	9	10	11		
11-Slice	Univariate	Multi-step	47.1	26.6	94.7	57.5	15.4	17.1	42	52	29.9	38.2	79.2	45.4	23.6
		Single step	54.5	26.2	51.5	26.2	29.4	29.3	49.6	40.6	45.1	37.7	81	42.8	15.6
6-Slice	Univariate	Multi-step	58.2	30.2	27.4	71.4	61.1	82.2						55.1	20.1
		Single step	63	20.5	28.5	46.6	60.4	90.9						51.6	23.4

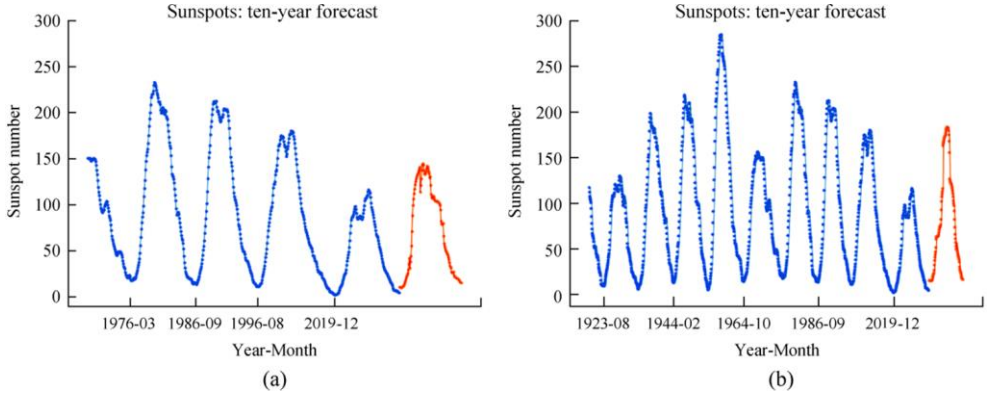

Figure 9: (a)11-slice and (b)6-slice predict the number of sunspots in the next 10 years.

ISSN 2616-5775 Vol. 6, Issue 13: 178-185, DOI: 10.25236/AJCIS.2023.061325

It can be seen from the experimental results that, in terms of prediction methods, whether it is shard 11 or shard 6, the prediction results of multi-step length are better than that of single step length. In univariate and multivariate comparisons, the multi-step square error of Shard 11 decreased from 43.1 to 42.8, a decrease of 0.3, and the standard deviation decreased by 3.5. For shard 6, although the multi-step multivariable prediction increased by 1.2, it can be seen from the results that the results of the second, third and fourth subsequences were significantly improved, but the errors of the first and sixth subsequences were too large, making the final mean root error greater than the multi-step prediction results of the single variable. To sum up, Shard 11 achieves the best results at the multi-variable optimal multi-step size, that is, when the step size is 6, it not only obtains a smaller mean square root error, but also the smallest root means square error standard deviation. Therefore, the Shard 11 result is considered more reliable, that is, the maximum amplitude of sunspots in the next 10 years is 144.9, which occurs in November 2035. The solar maximum lasts from May to 2037, lasting one year and six months.

4. Conclusions

This study's analysis and prediction of the sunspot activity cycle provide essential information for forecasting flood disasters. The use of Long Short-Term Memory Networks (LSTM-NN) effectively captures the nonlinear relationships in the sunspot time series, demonstrating strong predictive capabilities. Particularly, the LSTM model excels in addressing the issues of gradient vanishing and exploding, thereby ensuring the stability and reliability of the model. However, the study has limitations in addressing outliers in the time series data, which can be detected using methods like local correlation integrals. Additionally, the prediction of the solar cycle in the current model does not reflect the bimodal characteristics of the cycle, indicating a need for model improvement. These limitations highlight future research directions, including refining outlier detection and enhancing the model to capture more complex cycle characteristics, ultimately improving the accuracy and practical applicability of the predictions.

References

[1] Bi Chenglin, Liu Kuang, Xiang Zheng et al. Research on regional LSTM model of flood forecast [J/OL]. Hydropower Energy Science, 2023,(12):63-67[2023-12-04].
[2] Lu H, Yang F .Research on Network Traffic Prediction Based on Long Short-Term Memory Neural Network[C]//2018 IEEE 4th International Conference on Computer and Communications (ICCC).IEEE, 2018.DOI:10.1109/CompComm.2018.8781071.
[3] Zhu Xuefeng, Feng Zao, Ma Jun et al. Defect recognition model of Attention Mechanism U-shaped pipeline based on MSCNN-LSTM [J]. Journal of Vibration and Shock, 2023, 42(22):293-302.
[4] Zhang Wanting. Application of neural network method to solar activity index prediction [D]. National Space Science Center, University of Chinese Academy of Sciences, 2022. (in Chinese)
[5] Xu Hengyu. Long-term variation of sunspot asymmetry between north and south based on complex network [D]. Yunnan University of Finance and Economics, 2022.
[6] Wang X X. Simplified structure design of LSTM neural network and its application in effluent BOD prediction [D]. Beijing University of Technology, 2022.
[7] Yu N. Sunspot time series prediction based on multi-scale decomposition and particle swarm optimization of ELM [D]. Wuhan University of Science and Technology, 2022.
[8] Chen W. Correlation analysis of sunspot activity and sea level temperature [D]. Shanghai Normal University, 2022. (in Chinese)
[9] Ma F, Wang H X. Sunspot prediction based on NMPTS model [J]. Science and Technology Innovation, 2022, (05):189-192.
[10] Lv T , Wang Y , Yuan J ,et al. Prediction and Application of Network Business Traffic based on LSTM[J].IOP Publishing Ltd[2024-01-07]. DOI:10.1088/1742-6596/2289/1/012011.